Title: Co-fluctuations of neural activity define intra-V1 networks related to perceptual organization

Authors:

Mitchell Valdes-Sosa*[1,2], Marlis Ontivero-Ortega*[1,3], Jorge Iglesisas-Fuster[1], Agustin Lage-Castellanos[1], Lidice Galan-Garcia[1], Pedro Valdes-Sosa[2,1].

Affiliations:

[1] Cuban Center for Neuroscience, Havana, Cuba

[2] The Clinical Hospital of Chengdu Brain Sciences, University of Electronic Sciences and Technology of China, Chengdu, China

[3] Psychology Faculty, Ghent University, Belgium

* Both authors contributed equally

Email: mitchell@cneuro.edu.cu; luna@cneuro.edu.cu

Abstract

Using functional resonance imaging (fMRI), we studied the relationship between perceptual organization and network topology within the primary visual cortex (V1). Twenty-six humans (male and female) were recorded during active observation of two Global and Local Navon letters. Correlations between fMRI fluctuations from different V1 sites were measured (after removing stimulus-evoked signals) in windows specific to each condition. Intra-V1, like brain-wide networks, presented an overall decrease of correlations during stimulation compared to baseline but with increased statistical dimensionality. Massive edgewise testing and network based-statistics (both corrected by FDR) identified differences in connection strengths between stimuli that were mapped to the visual field. Global letters elicited long links mainly connecting V1 sites mapping the lower left/right visual quadrants. Shorter links were associated with local letters, primarily mapped within the lower-left visual quadrant. These connections were not observed in the time-locked (feedforward) responses shared across participants, and their lengths exceeded V1 population receptive field sizes. Thus, these networks reflect activity idiosyncratic to each participant, possibly generated by interactions within or feedback to V1. Perception would sculpt V1 connectivity, with specific increases in link strengths (in a background of decreases). These findings could help shed light on V1 as a "cognitive blackboard".

Keywords: V1, perceptual organization, connectivity, networks, fMRI

Running title: Within-V1 networks and perceptual organization

Introduction

The primary visual cortex (V1) is the main recipient of visual input from the retina and the initial station of specialized -feedforward- (Lamme & Roelfsema, 2000) neural routes enlisting higher-order visual areas (Goodale & Milner, 2018; Haak & Beckmann, 2016). In animal studies, V1 neurons have small receptive fields (RF) narrowly tuned for different stimulus features (Van Essen et al., 1984). Hence V1 acts as a bank of local feature detectors that provide a basic description of visual scenes (DeValois & DeValois, 1991). Consistently, the largest size of human V1 population RFs (pRFs) (Wandell & Winawer, 2015a), estimated with functional magnetic resonance imaging (fMRI), do not exceed 4-5º of visual angle in V1. Meanwhile, perceptual organization is a critical process that groups different stimulus elements, separates figures from the background, and establishes whole/parts relations. It also enables object-based attention (Kimchi et al., 2016; Pomerantz & Portillo, 2012; Wagemans et al., 2012). The stimulus elements to be grouped are frequently separated by distances much more extensive than pRF sizes in V1 (usually longer than 5 º). Thus, perceptual organization needs information integration across sizeable visual field sectors, which higher-order areas could provide with larger RFs (Christiaan Klink et al., 2021; Wandell & Winawer, 2015a).

Interestingly, there is evidence that V1 also contains information about stimulus organization and global properties, spanning distances longer than its small RF. Multivariate pattern analysis (MVPA) of fMRI in human experiments has produced evidence for global properties in V1. Scene identity can be decoded within regions of V1 that correspond to large, occluded parts of the visual field (Smith & Muckli, 2010). Information about object shapes presented in the periphery of the visual field can be decoded from the unstimulated foveal portion of the V1 (Williams et al., 2008). In addition to this increased spatial span, V1 can also

reflect purely top-down information. Thus, MVPA correctly predicts visual working-memory content from V1 activity without an exogenous stimulation (Harrison & Tong, 2009). This enriched V1 activity, not present in the classical RFs, could play an essential role in processes such as attention, working memory, and imagery, possibly acting like a cognitive blackboard (Roelfsema & de Lange, 2016a).

Interactions between different neuronal populations are needed to represent in V1 the large-scale -global- properties reviewed above. Local neural networks within V1 could play a role, with lateral connections between V1 neurons with similar edge-orientation selectivity facilitating the detection of extended contours (M. Chen et al., 2014; Kapadia et al., 1995; Liang et al., 2017; Schwarz & Bolz, 1991). But input from higher-order visual areas (Roelfsema & de Lange, 2016b) is required to make more complex features (e.g., object form or scene identity) and broader spatial coverage available to V1. Massive fiber connections from the visual higher-order regions to V1 could provide an anatomical basis for this feedback (N. T. Markov et al., 2011; Nikola T. Markov et al., 2014).

To understand the construction of the perceptual organization, we must measure cooperation between neurons scattered within V1, higher-order visual cortices, and beyond. Doing so is a daunting task. Luckily, this cooperation may imply the synchronization of neural activity (Singer, 2021). We could perhaps measure this synchronization in V1. Robust evidence indicates that brain sites with synchronized slow fMRI signals are parts of the same large-scale brain circuits (Bijsterbosch et al., 2017, 2020). Encouragingly for our purposes, fine-grained patterns of visual neural circuitry are also reflected by this activity. Connective receptive field (cRF) modelling uses the co-fluctuations of voxels in V1 with those in other cortical areas to estimate the equivalent of pRFs for the latter (Bock et al., 2015; Gravel et al., 2014; Haak et al.,

2013). Estimated cRFs correspond well with pRFs estimated with standard techniques. Voxel-to-voxel multivariate regressions (Baldassano et al., 2012) between V1 and target cortical areas have been used to estimate retinotopic mappings in the latter. The estimated maps fit closely with results from classical retinotopic mappings (Baldassano et al., 2016).

Therefore, the neural cooperation underlying perceptual organization could be partially reflected by co-fluctuations of fMRI activity between V1 sites. This idea was tested recently by Nasr and co-workers (Nasr et al., 2021) in an experiment with human subjects. Larger correlations were found between V1 regions of interest (ROIs) in different hemispheres when these areas mapped parts of the same object compared to when they mapped parts of different objects. This effect was stronger for stimuli in the lower visual field, congruent with a similar bias for global perception in human behavioral data (Nasr & Tootell, 2020; Previc, 1990). These results suggest that changes in perceptual organization are associated with modifications of functional connectivity within V1.

Here we followed up the study by Nasr and co-workers, using different stimuli and a finer anatomical scale. Global vs. Local compound (i.e., Navon) letters were used (Figure 1A), which induced attention to different spatial scales. Vertex-wise correlation of fMRI activity (between all cortical V1 nodes) was measured in time-windows corresponding to each type of stimulus. Furthermore, we propose a novel approach to performing intra-V1 connectivity analysis (pipeline in Figure 2). The goal was to identify reliable differences in intra-V1 correlation matrices across conditions, employing edge-based and network-based tests (Chung et al., 2021; Noble et al., 2022). Taking advantage of the close correspondence between V1 cortical anatomy and retinotopy (Benson et al., 2012; Benson & Winawer, 2018), we mapped onto the visual field those links between cortical sites that differed consistently between stimulus classes.

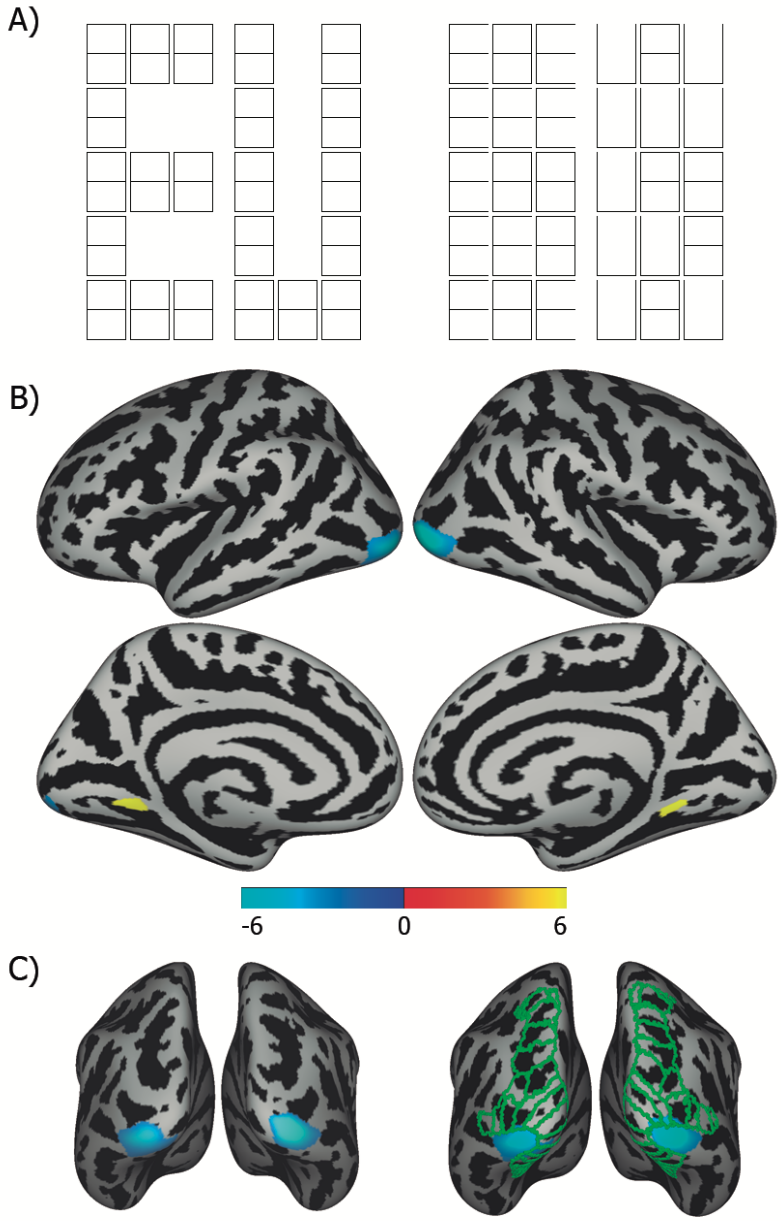

Figure 1. Stimuli and Global >Local activation maps. A) Examples of stimuli used in the experiment. From left to right, Global 'E' (EG) and 'U' (UG), Local 'E' (EL) and 'U' (UL). Black/white are reversed. Second-level activation maps (FDR threshold q=0.05), in B) lateral and medial views and in C) posterior views. On the right in C), green lines show the borders of retinotopic areas from the Wang et al. (2015) atlas. The Color bar corresponds to t-values.

We first verified if intraV1-networks presented two characteristics typical of brain-wide functional networks: correlation reductions accompanied by an overall increase in statistical dimensionality (thus less information redundancy) during task states compared to rest (Ito et al., 2020). We also hypothesized that V1 network topologies would reflect the perceptual organization of the observed stimuli, with the lengths and spatial distribution of the links in correspondence with the required perceptual windows of Global/Local letters (Han et al., 1999). Furthermore, it was predicted that V1 network visual-field mapping asymmetries would be analogous to the perceptual asymmetries present for this type of stimulus (Barbot et al., 2021; Kupers et al., 2019; Robertson & Ivry, 2000). Intra-V1 networks could be driven by feedforward responses shared across participants or activity idiosyncratic to each participant due to lateral interactions or feedback from other areas. We modelled task fMRI activity as a sum of components representing these different sources (Nastase et al., 2019). The weight of these components can be varied by appropriate preprocessing, which allowed us to assess their role in producing the studied networks.

Results

We examined the possibility that the topology of intra-V1-networks differed between modified Global and Local Navon letters, two classes of stimuli that differed radically in perceptual organization. With the modified Navon figures, temporal separation of the two levels is achieved, thus unmixing their fMRI responses. These stimuli were alternated with a background mask in 20 s blocks and presented in an MRI scanner to twenty-six participants. Local and Global versions of the "E" and "U" were used, and the participant's task was to count minor -and infrequent- deviations in letter shape (for more details, see Valdés-Sosa et al., 2020).

A second-level analysis for activations (FDR corrected, q=0.05) was performed as a control. Increased activity was found in the foveal V1 for Local -compared to Global- letters (Figures 1B and C). Previous work has explained this localization by a more restricted spatial focus of attention for local attention (Sasaki et al., 2001). An increase in activity within a small region in the para-hippocampal cortex was also found for Global -compared to Local- letters.

V1 network analysis pipeline

V1 connectivity matrices were obtained for condition-specific fMRI activity using the pipeline depicted in Figure 2. In each participant, the fMRI time series were projected from their native volume to their cortical surface and subsequently registered to the FreeSurfer average surface. A group of nuisance variables was regressed out of the fMRI time series to eliminate the effects of noise, artifacts, and physiological contaminants. The primary analysis was carried out on background activity, defined as the residual time series after regressing out the stimulus-evoked activity. The stimulus-evoked activity was modelled by convolving the SPM canonical hemodynamic response function (HRF) with the timing of the stimuli (no-deconvolution and deconvolution with finite impulse responses, FIR, were also tested). Time segments related to the

same condition were identified (after accounting for the HRF delay) and concatenated. The Pearson correlations between all V1 surface vertices were calculated.

The second-level connectivity analysis consisted of contrasts between the matrices from different stimulus conditions. Subtracting correlations minimizes the effect of between-site geodesic and retinotopic-eccentricity separation, which otherwise would dominate V1 connectivity estimates. Two within-subject statistical approaches were used. The first consisted of massive univariate t-tests on the connection (edge) strengths, with correction for multiple testing through false discovery rate (FDR, q=0.05) thresholds. FDRs were estimated for both tails of the t-value distribution by using mixture modelling (Bielczyk et al., 2018; Gorgolewski et al., 2012). Edgewise analysis has the advantage of greater spatial precision but also less statistical power (Noble et al., 2022). Secondary statistics were derived from the networks sparsified with FDR thresholds. For this we used ten geometric definitions of links (e.g., links crossing the vertical meridian in the lower visual field, see Figure 7 for cartoons illustrating each case), which we dubbed connectivity subspaces or connSubsp.

In addition to edge-based analysis, we used constrained network-based statistics -cNBS- (Noble and Scheinost, 2020), which is less precise spatially but has more statistical power. This method uses as input the edge-based tests. It also requires an “a priori” (independent) partition of the correlation matrix into sub-networks for which summary statistics are generated and submitted to permutation tests. Here we used the same subdivisions described above (connSubs). Finally, three additional variants of Step B from Figure 2 (before calculating the correlations matrices) were used to explore the neural sources of V1 networks, as described in another section.

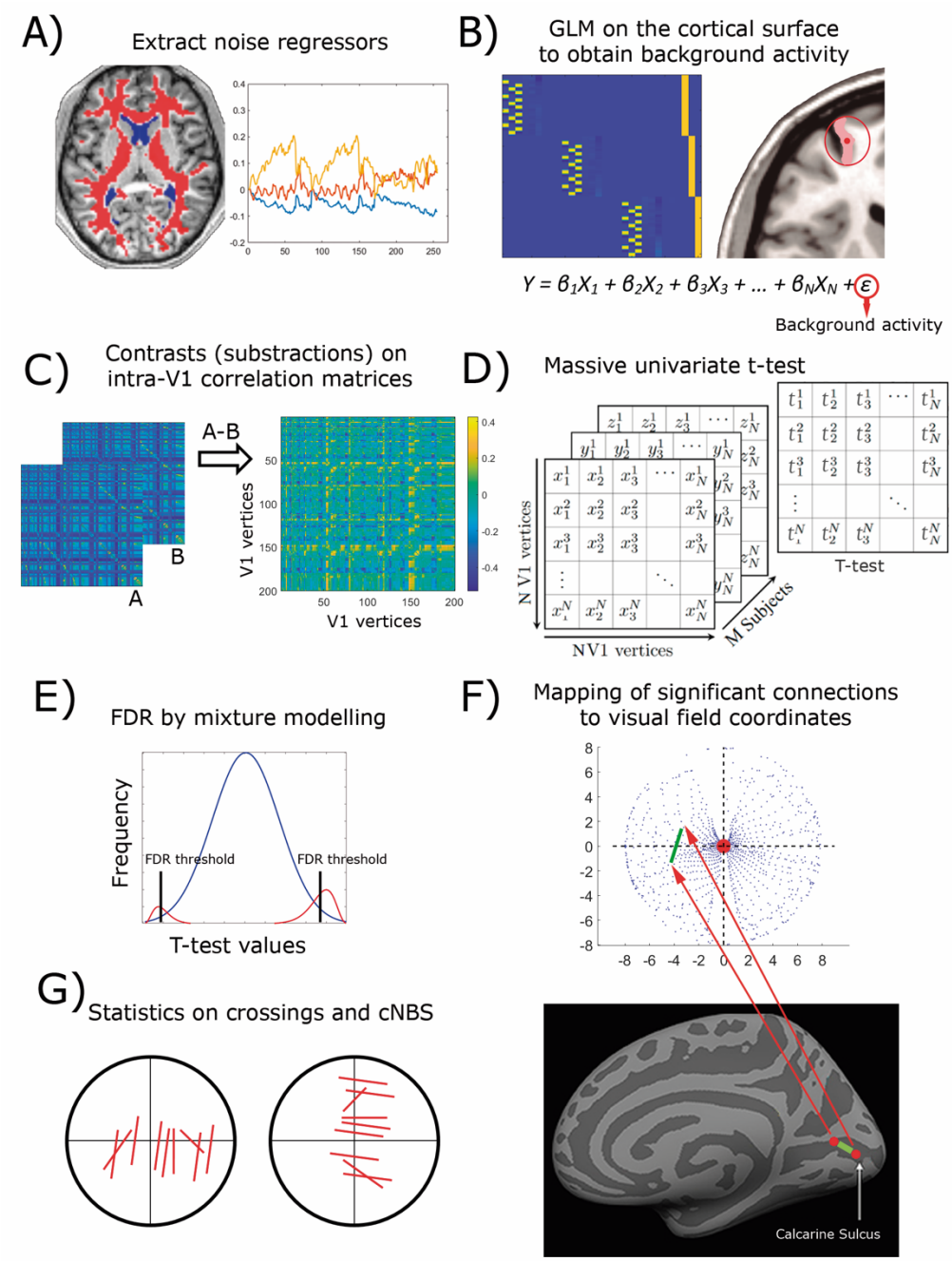

Figure 2. Primary data analysis pipeline. A) The first five principal components of white matter and ventricular (red and blue respectively in the image) time series (and derived measures) were extracted from the volume fMRI data. B) A general linear model on cortical surface data was used to regress out the contributions of the noise parameters, motion correction parameters (and derived measures), and the stimulus-evoked activity. C) The resulting background activity was windowed to correspond with stimulus effects (considering the hemodynamic response lag), and correlation matrices between all V1 cortical vertices were

obtained per subject, Fisher transformed, and (depending on the contrast) subtracted to produce difference matrices. D) A massive univariate t-test was performed on each entry in the difference matrices across subjects. E) Mixture modelling of the t-values was used to obtain false discovery rate thresholds, illustrated here by a Gaussian null (blue) and two gamma functions (red). F) Connections on the cortex that survived the FDR thresholds were mapped to visual field coordinates (see red arrows), using population values for the pRF centers of each V1 cortical vertex (blue dots). An example of a between-vertex link is shown in green on the inflated cortical surface on the visual field. G) Several statistics were measured on the significant connections, including the number of crossings through the horizontal (left) and vertical (right) meridians. Network-based statistics were also calculated.

Plausibility check of pipeline results

Given the multiple opportunities for processing errors in the pipeline, we conducted a plausibility check based on two network attributes predicted by previous work. First, intra-V1 correlations between sites decrease with their separation on the surface (Dawson et al., 2016). As seen in Figure 3 A, the final output of our pipeline is consistent with this finding since between-site separation has a sizable effect on the correlations. Polynomial fits to these curves were slightly different across conditions ($y=3.25*x^{-0.75}$ with R2=0.85 for the Local, and $y=3.23*x^{-0.74}$ with R2=0.82 for the Global letters). The dominant influence of geodesic distance on inter-site correlations validates our strategy of subtracting measures between conditions for each edge to eliminate this effect.

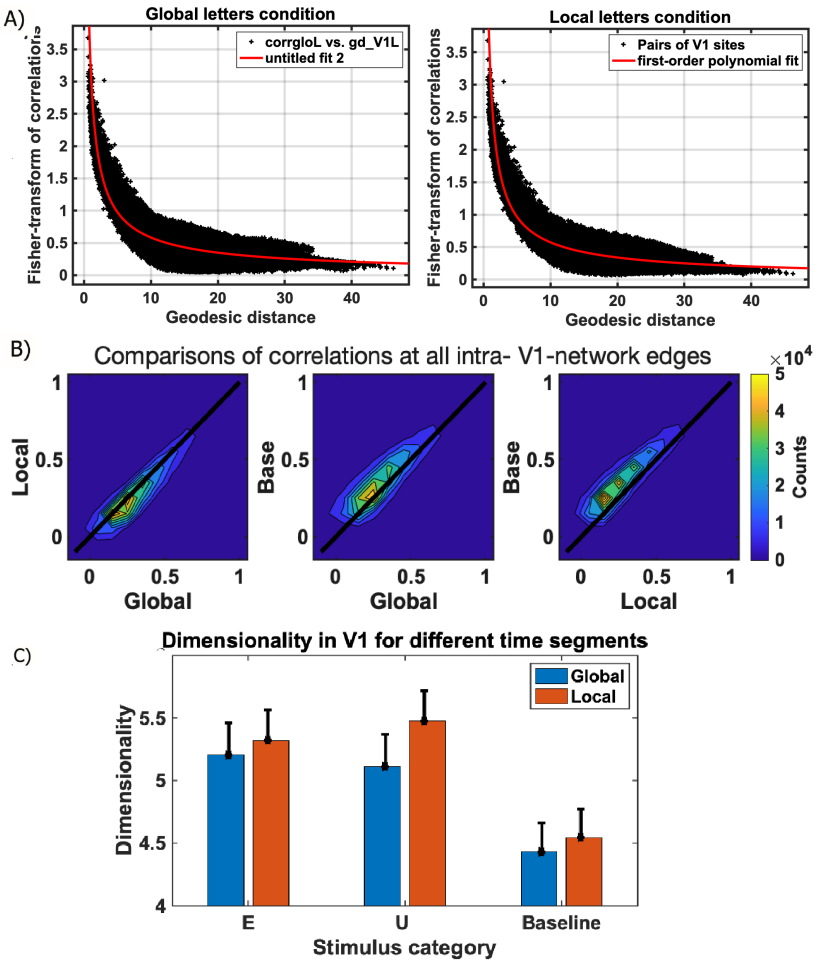

Figure 3. Pipeline plausibility check results. A) Between-site correlations in the left V1 as a function of their geodesic separation over the cortical surface. A first-order polynomial regression fit to the data is shown as a black curve for each condition. B) The 2D histograms of V1 of binned correlations for pairs of stimuli across all edges in V1. The black diagonal line indicates identical correlation values. C) Dimensionality for different V1 covariance matrices.

Second, there are consistent reports that correlations in brain-wide functional networks are significantly smaller for task fMRI than in the resting state (Ito et al., 2020). This reduction was also found in intra-V1 networks (Figure 3B). The correlations obtained for fMRI measurements from the Baseline before each stimulation block were larger than for the Global and Local segments at 76% and 70 % of the edges, respectively. The advantage for the baseline

were significant in paired t-tests on z-transformed correlations for all V1 edges ($t(349029)=271.3$, $p<0.00001$ for Global, d=and $t(349029)=429.5$, $p<0.00001$ for Local letters). There was also a significant ($t(349029)=,271$, $p<0.0001$), albeit less pronounced, advantage for Global over Local letters (in 24% of edges). Measures of Cohen's d confirmed this pattern. The effect size was moderate (0.72) for the Baseline>Global, strong (1.6) for Baseline>Local, and small 0.45) for Global>Local comparisons.

The statistical dimensionality of the covariance matrices associated with each stimulus, and the baseline segments preceding them (segregated by the level of the subsequent letters), is shown in Figure 3C. Higher dimensionality was found for matrices related to Global $F(2, 50)=13.0$,$p=0.0013$) and Local ($F(2, 50)=16.5$, $p=0.0004$) letters compare to both baselines. There was no effect of letter identity, letter level or their interaction on dimensionality. A nonsignificant trend to slightly smaller values for Global relative to Local was seen (although this should be defined with properly powered studies).

Topology of intra-V1 networks associated with Global/Local Navon Letters

The results of the connectivity analyses after canonical-HRF deconvolution are shown in Figure 4. Both classes of stimuli produced reliable V1 networks. Figure 4A shows that FDR thresholds were found at both tails of the distribution of t-values. This probably is because well-defined objects (well separated from the background) were present in both conditions that elicited distinct network topologies. The link maps in the visual field (Figure 4B) show clear network topology differences between the two conditions. It is evident that for the Global condition, numerous links connected the left and right visual hemifields, especially for the lower visual quadrants. These horizontal –left/right- links were absent for the local condition, for which most network edges started and ended within one quadrant, especially in the inferior right

quadrant. In Figure 5, Cohen's d estimate of effect size is displayed for each link that presented values above 0.5. This figure suggests that many links with moderate to large effect sizes failed to reach the FDR, which tends to be conservative. We performed the network-based analysis described below to overcome this limitation of edgewise analysis.

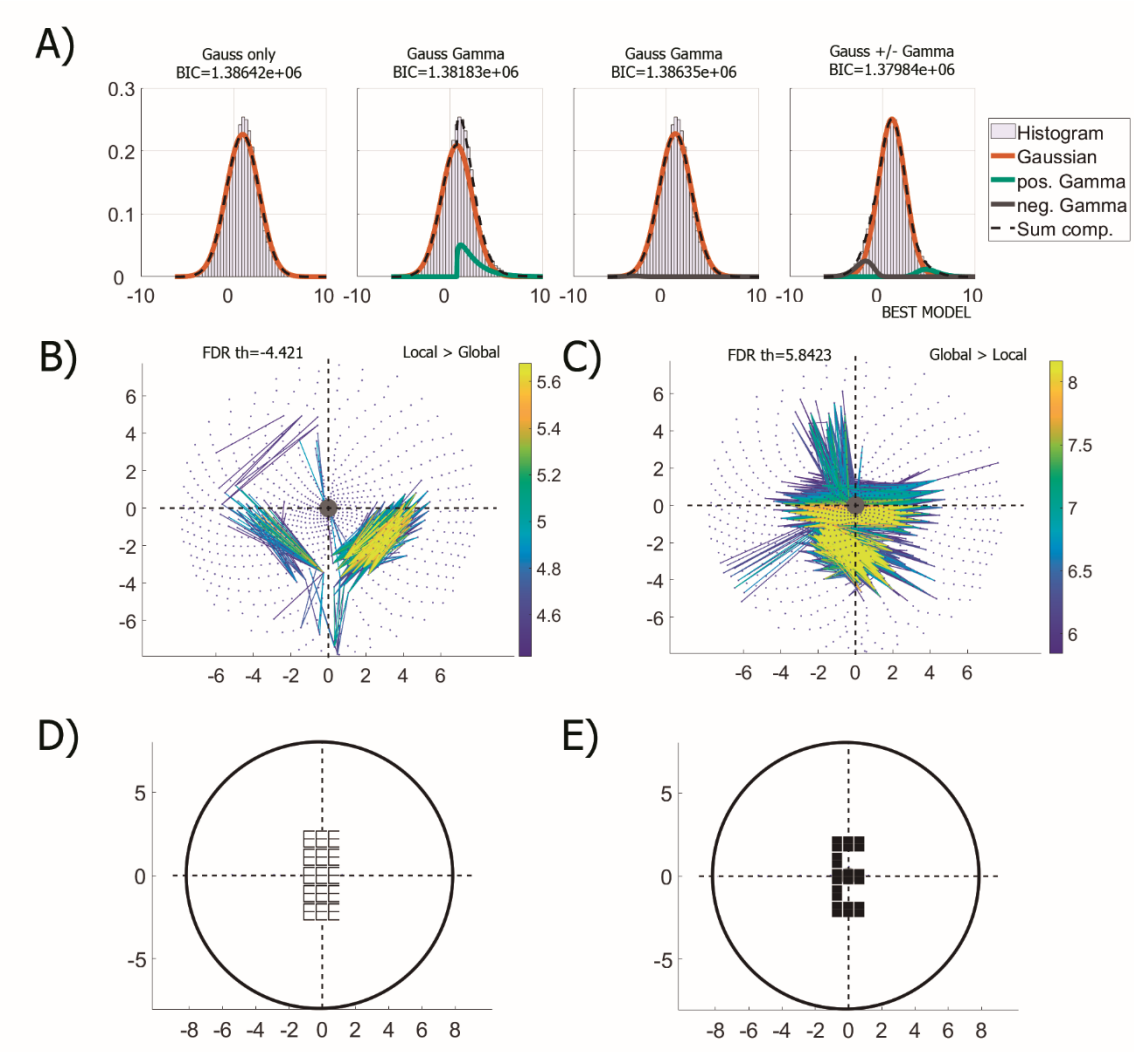

Figure 4. A) Distribution of t-values and mixture models fits. BIC values are displayed above each mixture model. B) Plot in the visual field of connections surviving the FDR threshold (q=0.05) for Local>Global contrast, C) for the Global>Local. Blue dots are pRFs centers for each V1 vertex. FDR threshold in insets. The lines join the two centers in a significant link, with a color code for their absolute t-value. D and E) Approximate size of stimuli in the visual field.

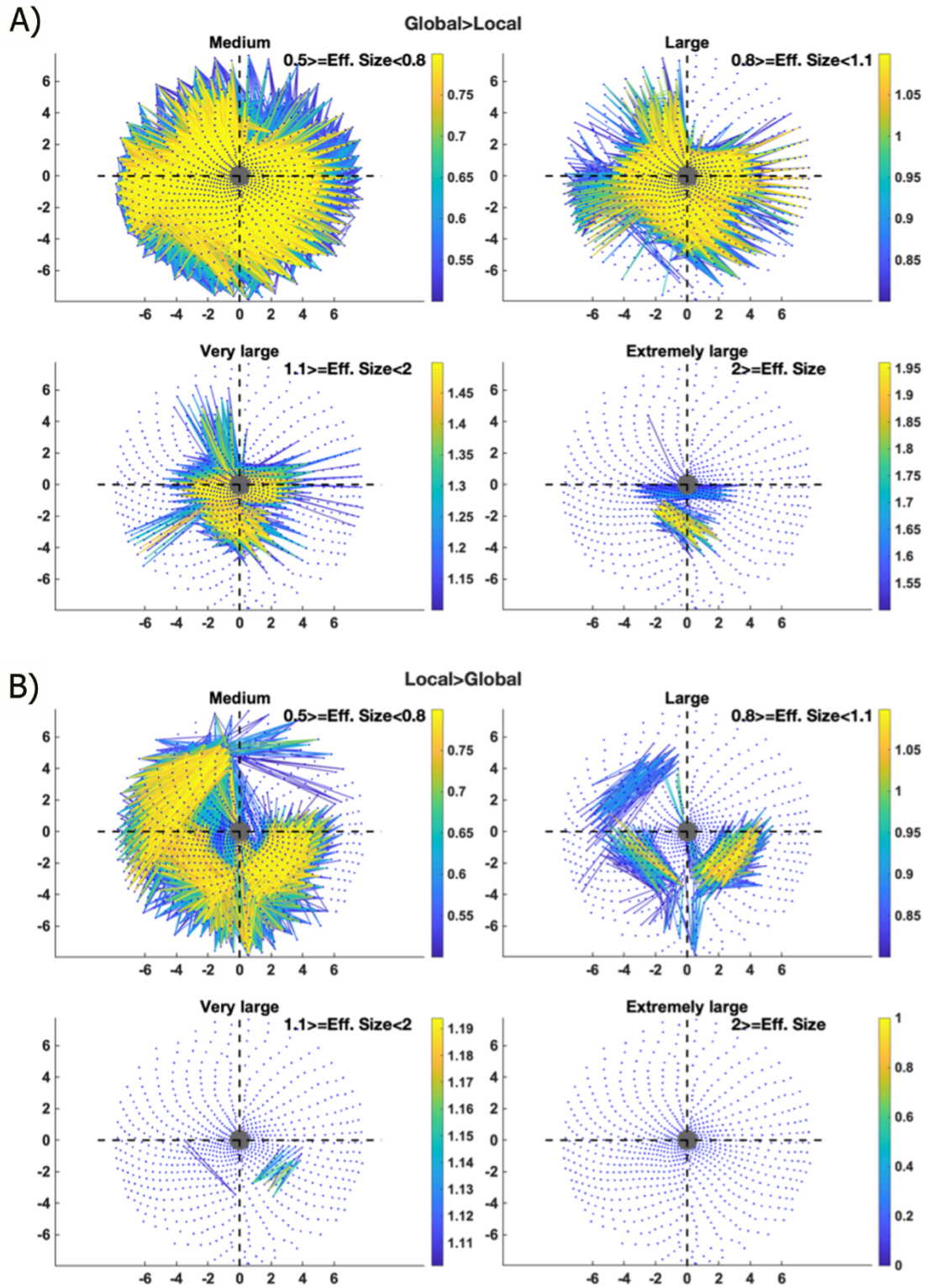

Figure 5. Effect sizes (Cohen's d) for the V1 links for each contrast (no vertex-wise FDR thresholding). The maps are sorted according to effect size ranges as indicated in the insets. Only d > 0.5 are shown. A) Global>local. B) Local>Global.

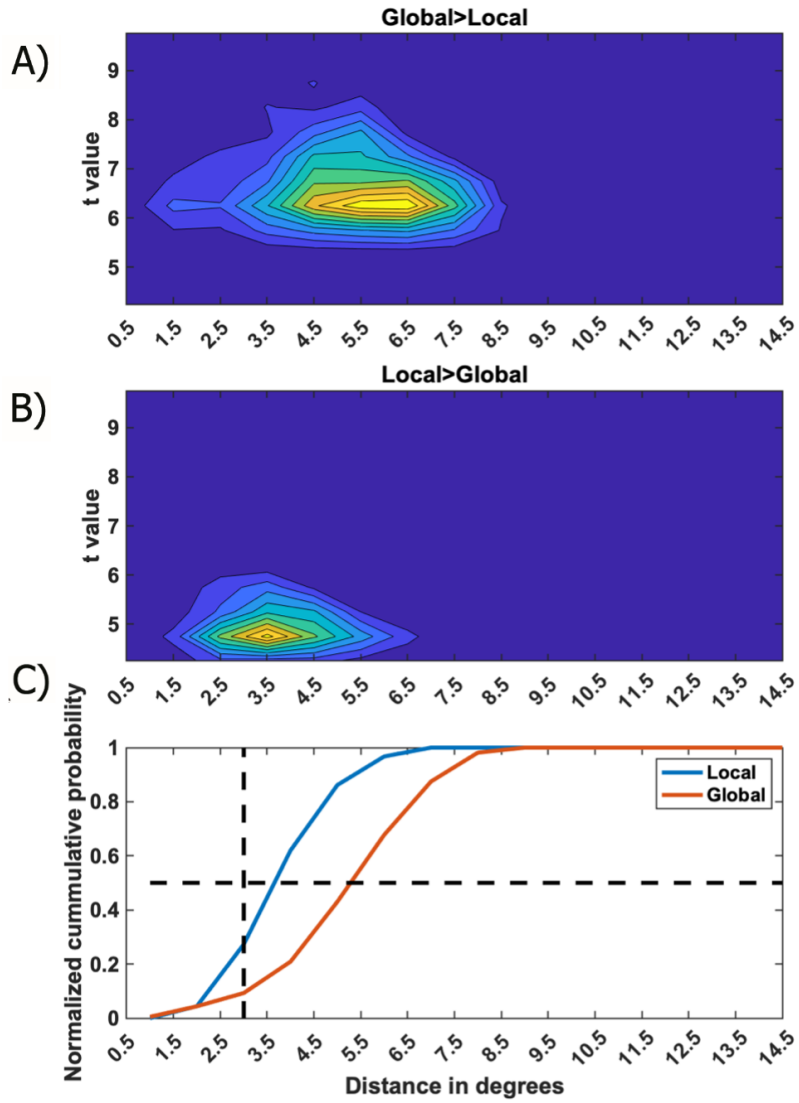

Figure 6. Histograms of link t-values and lengths in the visual field. A) 2-D histogram of link lengths and t value counts for elements surviving the Global>Local FDR threshold; B) 2-D histogram of link lengths and t value counts for elements surviving the Local>Global FDR threshold. C) Normalized cumulative histogram of distances for links in A) and B). The vertical black dashed line corresponds to maximum pRF sizes in V1 for the central 8 degrees of eccentricity. The horizontal line corresponds to the 50% accumulation level (medians).

Significant connections tended to be longer in visual field space for the Global>Local contrast (median= 4.5º) than for the Local>Global contrast (median= 3.6º) (Figure 6). This

difference in distributions was highly significant in a Kruskal-Wallis test (df=1, Chi-sq=3.6471e+03, $p<0.0001$). Note that the t-values are larger also for the Global compared to the Local conditions. Furthermore, the median length for both types of stimuli was larger than 3º of the visual field, which is the maximum pRF size in the areas of V1 mapping the central 8º of the visual field (Wandell & Winawer, 2015).

The same analysis after no-deconvolution allowed FDR threshold estimation. The networks were like those described above but with fewer significant links in each condition. The distribution mixture models did not yield FDR estimates after deconvolution with FIR.

Visual field asymmetries of intra-V1 networks

We measured the proportion of significant connections that crossed from one visual quadrant to another or stayed in the same quadrant for each stimulus condition (Figure 7). For this, we designed a basis of orthogonal sub-spaces of connections (connSubsp, see top row Figure 7), in each of which the number of significant connections was counted. Connections for the Global>Local case mainly crossed the vertical meridian, linking the left and right visual hemifields (i.e., V1 from the two cerebral hemispheres), with many more connections in the lower quadrants. There were also diagonal and antidiagonal connections between the left/right hemifields. There were few links in other regions, with only a few links connecting the upper and lower quadrants on the left side.

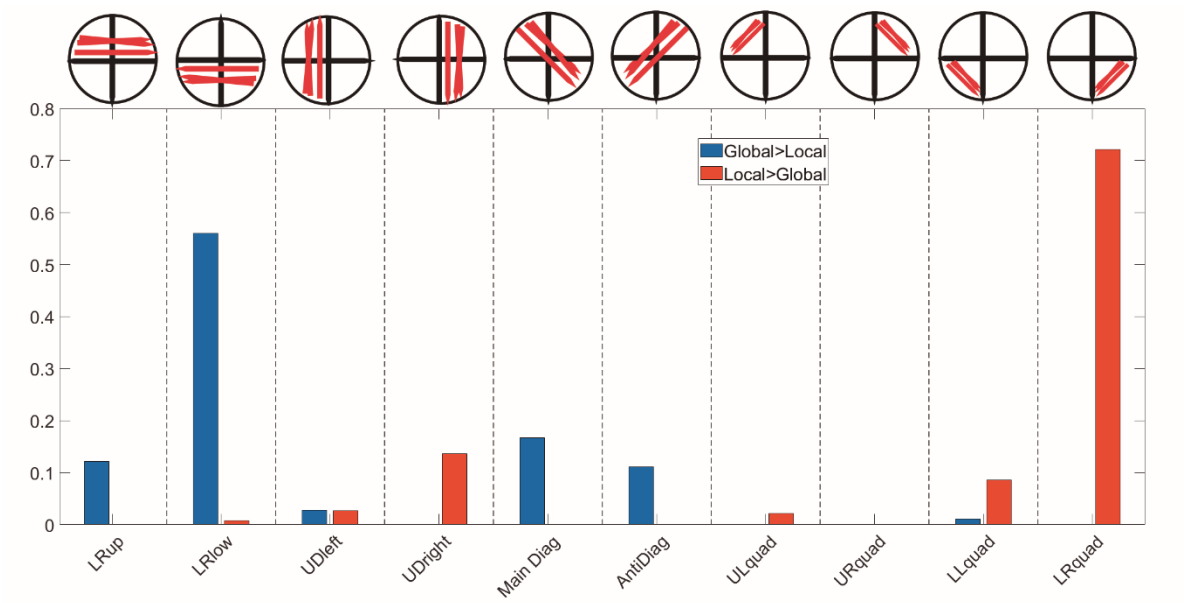

Figure 7. The proportion of connections between/within visual quadrants. Insets schematize type of connection (connSubsp groups) that were also used in the network-based analysis. LRup and LRlow, left-right crossings in the upper and lower hemifields. UDleft and UDright, up-down crossings in the left and right hemifields. Main Diag and Antidiag are diagonal links. URquad, ULquad, LLquad, and LRquad, are the links limited to the upper-right, upper-left, lower-left and lower-right visual quadrants.

This contrasted with the Local>Global case, in which almost none of the connections crossed the vertical meridian. In the latter condition, most connections stayed within the lower right quadrant, with a smaller number in the lower left quadrant. There were also links between the upper and lower quadrants on the right side of the visual field. Thus, perceptual organization influenced both the strength and length of connections strengths in V1 and the spatial pattern of links between (and within) visual quadrants. Using a Fisher exact test, we found significant differences between the Global and Local conditions in the proportion of left-right crossings in the lower visual field ($p<0.0001$), up-down crossings in the left hemifield ($p< 0.023$), up-down in the right (p,0.0001), crossings staying within the lower left ($p<0.0001$) and lower right quadrants ($p<0.0001$).

312 Each preprocessing scheme differentially suppresses fMRI sources

313 We modified the fMRI preprocessing steps to explore which fMRI components
314 contributed most to the V1 networks described here. The stimulus sequence and timing were
315 identical for all participants. Hence, it was possible to model the fMRI signal at each cortical
316 vertex as the sum of four sources, according to the following equation (modified from Nastase et
317 al., 2019):

318 $$Y(stim, sub) = C(stim) + IdPl(stim, sub) + IdNpl(stim, sub) + N(sub) \quad (1)$$

319 Where *stim* is the stimulus, *sub* is the participant, *Y* is the fMRI time series, *C* is the response
320 shared across participants, *IdPl* is the idiosyncratic phase-locked response to the stimuli, *IdNpl* is
321 the idiosyncratic non-phase-locked response (i.e., modulation of the "intrinsic" or "background"
322 activity), and *N* are the noise components. In all analyses, the contribution of *N* was first reduced
323 by regressing out nuisance covariates, thus the denoised raw data would mainly contain the first
324 three terms of equation 1. Table 1 shows how the fMRI preprocessing procedures used in this
325 article theoretically suppress specific components. This was verified with spectral analysis of the
326 fMRI time series as described below.

327 **Table 1.** Effects of preprocessing on fMRI sources for intra-V networks.

Components contributing to correlations after each preprocessing strategy			
	$C(stim)$	$IdPl(stim, sub)$	$IdNpl(stim, sub)$
ISC	Keep	-	-
No-deconvolution	Keep	Keep	Keep
Deconvolve with Canonical HRF	-	Keep	Keep
Deconvolve with FIR	-	-	Keep

328 Here, intersubject correlations (ISCs) were obtained by averaging the fMRI time series at
329 one V1 cortical vertex across n-1 participants and then calculating the correlations with the time
330 series of the other vertices from the left-out participant. This produced n correlation matrices that

were averaged. This procedure only leaves the shared response C. In no-deconvolution, responses to task events were not regressed out, thus keeping the first three terms of equation 1. In contrast, deconvolving task-events with the canonical HRF described above (which has been used in previous studies of connectivity in task fMRI (Keller et al., 2022; Tran et al., 2018)), suppresses C leaving $IdPl\ and\ \ dNpl$. This is because the canonical HRF captures C variance well, as demonstrated by large correlations (between 0.8 and 1 across V1 sites) between the grand-average of time series across subjects with the predicted time course obtained with this HRF. Deconvolving response to task-events with a finite impulse responses basis (FIR) suppresses C and $IdPl$, the phase-locked components (Årup et al., 2000; Kay et al., 2008), leaving only $dNpl$.

This characterization of the effects of different preprocessing strategies (Table 1) is sustained by the power spectra of the time series they produce (Figure 8). Stimulation blocks for the Navon letters lasted 44 s; thus, the fundamental frequency was approximately 0.023 Hz. The Grand average (dominated by the C component) presents large peaks at this frequency, its harmonics, and the subharmonic (problem arising from aliasing). These peaks are small in the raw data, smaller after de-convolution using the canonical HRF, and smallest when deconvolving with FIR, a decrement which probably reflects the progressive removal of phase locked event related responses.

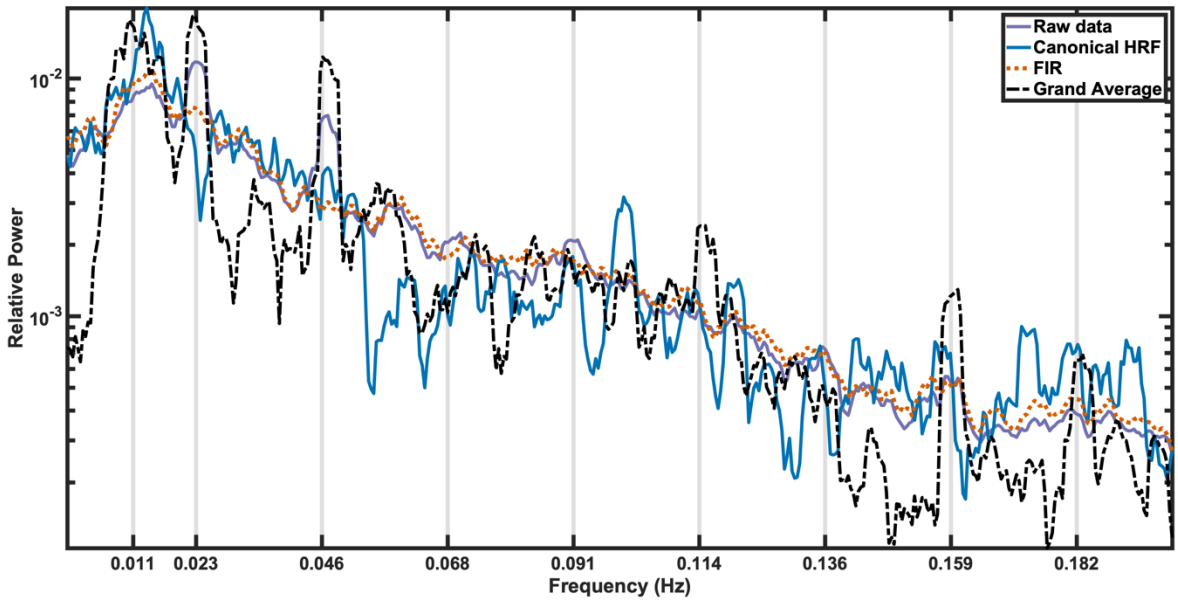

Figure 8. Relative power spectra of fMRI recordings. Each curve represents a different preprocessing strategy. All spectra were calculated after denoising. The vertical gray lines represent the fundamental frequency of stimulation (1/44 s), the first 7 harmonics, and the 0.5 sub-harmonic. Grand average is the spectrum of the time series averaged across subjects. Raw is the average for the spectra from all participants when the stimulus response was not de-convolved. Canonical HRF is the average of the spectra from all participants after the stimulus response was regressed out from the denoised raw signal.

cNBS analysis

We confirmed these results obtained with edge-based analysis, and compared the topologies found after different types of preprocessing by using a constrained network-based statistic (cNBS), which has increased power compared with other methods for testing hypotheses about networks (Noble et al., 2022). This approach requires independently defined subnetworks to avoid circularity, which is achieved with the connSubsp groups. The cNBS for each connSubsp group was defined as the mean t-values of the links belonging to the group from the Global Vs. Local contrast, in which only vertices in the central 4° of eccentricity were included. The probability of the observed cNBSs belonging to a null distribution centered on zero was

estimated in a permutation test. The null distribution was created by randomly flipping the signs of each participants correlation differences 10,000 times and recalculating the cNBS. The results of the tests are shown in Table 2.

Table 2. cNBS permutation test results as a function of preprocessing type. Entries are probability of belonging to the null distribution. With Bonferroni correction p=0.05 is 0.0045.

	ISC.		No deconv.		Canonical-HRF deconvol.		FIR deconvolv	
Row	G>L	L>G	G>L	L>G	G>L	L>G	G>L	L>G
LRu	0.3485	0.6516	**0.0001**	1.0000	**0.0001**	1.0000	**0.0001**	1.0000
LRlo	0.8858	0.1143	**0.0001**	1.0000	**0.0001**	1.0000	**0.0001**	1.0000
UDle	0.6369	0.3632	1.0000	**0.0001**	0.9994	**0.0007**	0.9997	**0.0004**
UDr	0.1718	0.8283	0.9995	**0.0006**	0.9978	**0.0023**	0.9998	**0.0003**
ULeq	0.6667	0.3334	1.0000	**0.0001**	0.9983	**0.0018**	0.9996	**0.0005**
URq	0.0047	0.9954	0.9988	**0.0013**	0.9998	**0.0003**	0.9999	**0.0002**
LoLeq	0.5521	0.4480	0.9999	**0.0002**	1.0000	**0.0001**	0.9998	**0.0003**
LoRq	0.1116	0.8885	0.9949	0.0052	0.9748	0.0253	0.9991	**0.0010**
DiagP	0.6262	0.3739	**0.0001**	1.0000	**0.0001**	1.0000	**0.0001**	1.0000
DiagS	0.9178	0.0823	**0.0001**	1.0000	**0.0001**	1.0000	**0.0001**	1.0000

It is clear from this table that, the cNBS analysis confirms the edgewise analysis for the time series deconvolved with the classic HRF (compare with Figures 5 and 6), and extends the results when the stimulus-evoked activity was not deconvolved or when it was caried out with a finite impulse response (FIR) basis. In contrast, ISC (representing the activity common to all subjects) did not generate the same pattern, with no tests surviving the Bonferroni correction This analysis was confirmed by estimates of the effects size of the cNBS, where there was a tendency for reduced effects sizes in the following order: no deconvolution, deconvolution with the classic HRF, deconvolution with FIR and ISC.

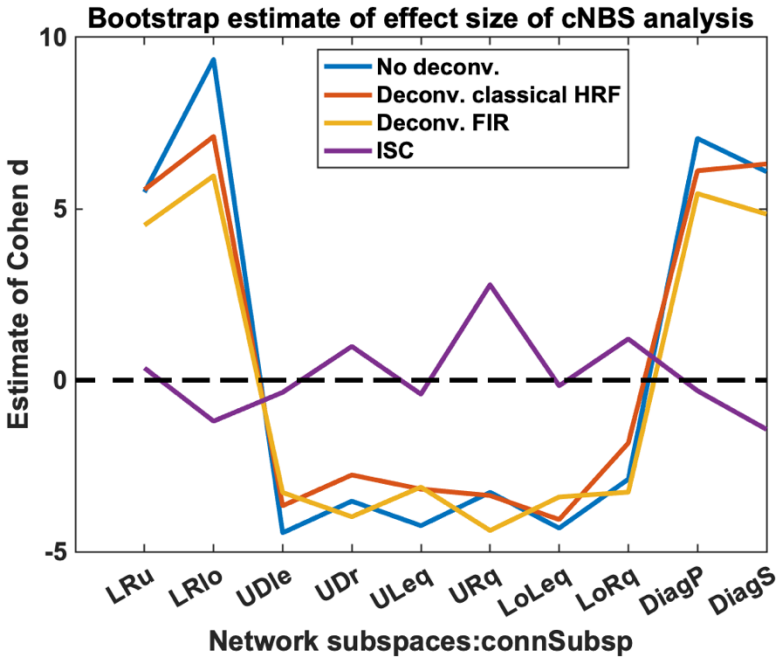

Figure 9. Estimates of effect sizes of the cNBS analysis for Global-Local contrast. Cohen's d was estimated by bootstrapping the cNBS (resampling participants with replacement, n=1000). Positive values indicate larger cNBS values for the Global condition, and negative for the Local one.

Discussion

Intra-V1, like brain-wide networks, presented an overall decrease of correlations during stimulation compared to baseline but with increased statistical dimensionality. We also found that the pattern of synchrony of neural activity between V1 cortical nodes varied systematically with re-configurations in perceptual organization. Compared with Local letters, Global Navon letters were associated with longer connections in the visual field, frequently crossing the vertical meridian, especially in the lower visual field. In contrast, links related to Local letters were shorter and restricted mainly to the lower right visual quadrant and infrequently crossed the vertical meridian. These effects were not seen with intersubject correlations and were weaker if deconvolution of the stimulus-related response was not carried out.

Before discussing the main results, it is necessary to consider if the intermediate outputs of our pipeline are credible according to prior knowledge. Each step in the pipeline is an opportunity for a mishap. Three results suggest that the outputs are adequate for our purposes. Firstly, we found that intra-V1 correlations decrease with greater separation between cortical nodes. This is congruent with other studies (Dawson et al., 2016; Raemaekers et al., 2014), that additionally found lower correlations if the mapped eccentricity of the sites has larger discrepancies. This justifies focusing on differences between correlation matrices to circumvent the dominant effect of between-site distance, which is constant. Retinotopic mapping is also roughly stable, although may change somewhat with the task (e.g., Kay et al., 2015).

Secondly, we found decreased correlations during stimulation -compared to a baseline mask- and increases in statistical dimensionality measures within V1. The same outcome has been reported in previous studies of brain-wide networks using large datasets (Ito et al., 2020), with a reduced correlation between brain regions, accompanied by an increase in dimensionality

(indicating less information redundancy) during task states compared to resting state. This has been suggested to facilitate increased information coding capacity. Thirdly, the peaks of V1 fMRI power spectra have the typical 1/f slope and change as predicted when the stimulus-evoked response is eliminated.

The edgewise and the network-based analyses produced compatible results, each at its predesigned spatial scale. Without evoked-response deconvolution, and when it was carried out with the canonical HRF, it was possible to adequately estimate FDR thresholds, something not achieved for FIR deconvolution. In the latter case, smaller responses (and poorer signal/noise ratios) were probably responsible for this failure. This supports the idea that mass univariate testing followed by correction for multiple comparisons may be too conservative and only allows us to see the "iceberg tip" among results (G. Chen et al., 2022). This conclusion is reinforced by a comparison of the FDR thresholded t-maps with their corresponding effect size maps. The meagre t-maps only exhibit extreme Cohen d values, while missing links with strong effects (e.g., from 1.1 to 2 for Global stimuli). However, the t-maps (especially for canonical HRF deconvolution) allowed a precise visualization of significant links. While conducive to less precise localization, the greater statistical power of cNBS verified that the same sub- networks were significantly different between the Global and Local conditions for all preprocessing schemes except ISC. The corresponding sub-networks contained the significant links from the edgewise analysis,

Our results are congruent with those reported by Nasr and co-workers (Nasr et al., 2021), the only previous fMRI study exploring the influence of perceptual organization on intra-V1 connectivity to our knowledge. In both studies, the synchrony of fMRI activity between the left and right V1 sites increased when they mapped parts of the same object compared to parts of

431 different objects. In our case, the Global letters straddled the vertical meridian of the visual field,
432 and neural activity from both hemispheres was needed to perceive their overall shape. Like the
433 fragmented condition in Nasr et al., most of our local letters were circumscribed to either the left
434 or right visual hemifields, making interhemispheric integration unnecessary for their perception.
435 This could explain the paucity of left/right links in this case. Compound figures are perceptually
436 segregated into smaller elements when processing local letters (Han & Humphreys, 2010),
437 consistent with the short, quadrant-constrained links described here for this condition.

438 Moreover, in both studies, the interhemispheric connections associated with Global
439 stimuli were stronger in dorsal V1 (i.e., the lower visual field). It has been argued that visual
440 perception is more Global for stimuli presented to the lower than the upper visual field
441 (Christman, 1993; Levine & Mcanany, 2005; Previc, 1990). This asymmetry could be related to
442 a greater sensitivity in the lower visual field to lower spatial frequency (SF) components.
443 Relatively lower SF components are critical for extracting the Global shape in Navon figures,
444 whereas higher SF components play a more significant role in the perception of local shapes
445 (Flevaris & Robertson, 2016). The neural basis of this vertical asymmetry has been recently
446 examined (Nasr & Tootell, 2020).

447 We found that local letters were related to links restricted to the lower right visual field,
448 which projects to the left hemisphere. When local Navon letters are briefly flashed
449 simultaneously in both visual hemifields, the right-sided letters are reported faster and more
450 accurately than the left-sided ones (Flevaris et al., 2010). This is congruent with studies showing
451 that patients with left hemisphere lesions perform worse on recognition of local Navon letters,
452 compared to cases with right hemisphere lesions (Robertson et al., 2010). This is also consistent
453 with reports that attending to local Navon letters elicits larger event-related potentials over the

left side of the scalp (Han et al., 2002; Iglesias-Fuster et al., 2014; Jiang & Han, 2005). The inverse patterns are found for Global Navon letters, which leads to the hypothesis that the left/right cerebral hemispheres are specialized for Local/Global processing (Flevaris & Robertson, 2016; Han & Humphreys, 2010).

However, in contrast to Nasr and co-workers, we also found stronger correlations between dorsal and ventral V1 from the same hemisphere (corresponding to the lower and upper visual fields) for Local compared to Global Navon letters. This could reflect horizontal neural binding for these stimuli. The reason for this discrepancy is unclear, but two explanations should be explored. First, we employed a more exhaustive set of nuisance covariates than Nasr et al. to reduce noise in the fMRI time series as is now standard in studies of functional connectivity (e.g., Cole et al., 2021). When this procedure was omitted, our network effects lost statistical significance. Second, we used actively attended foveal stimuli, whereas unattended peripheral stimuli were used in Nasr et al. The latter approach could weaken V1 functional links crossing the horizontal meridian.

Different fMRI preprocessing approaches allowed us to narrow down the possible sources of the observed V1 networks. The feedforward response to the stimuli (*C*) shared among participants (Nastase et al., 2019) does not contribute to the intra-V1 networks described here. Although the leave-one-subject-out procedure we used to calculate ISC can inflate positive findings (Chen et al., 2016), we found the opposite result: none of our network effects were verified with intersubject correlations. Furthermore, even with the high power cNBS method the analysis based on ISC does not evince the networks. Contrariwise, the networks are present after deconvolution with the canonical HRF or with FIR (procedures that suppress *C*). Thus, the network effects probably arise from activity idiosyncratic to the participants. Participant

idiosyncratic activity can be phase locked to the stimuli (e.g., fluctuations in evoked activity) or non-phased locked (e.g., spontaneous oscillations, also known as background activity).

A second clue to the neural sources of the networks is the length of significant links when mapped onto the visual field. These lengths exceed the size of the largest pRFs in V1 (Benson & Winawer, 2018; Wandell & Winawer, 2015b). Hence, the co-fluctuations of neural activity we observed in V1 are not due to a stimulus being encompassed within individual pRFs. This points to lateral interactions within V1 (Kapadia et al., 1995; Liang et al., 2017) or feedback from higher-order visual areas with large RFs (Briggs, 2020; Williams et al., 2008; Yukun, 2016) as an explanation. There is evidence for both mechanisms. It is thought (Field & Hayes, 2004; Kuai et al., 2017; Schwarz & Bolz, 1991) that enhanced co-activation of neurons in V1 via lateral connections in its superficial layers would facilitate the detection of extended contours. Moreover, microelectrode recordings in monkeys suggest that contour detection emerges first in V4 and then is fed back to V1 neurons (Chen et al., 2014), with V4 modulating V1 lateral interactions (Liang et al., 2017). Ultrahigh-field layer-specific fMRI studies in humans have found effects of Global stimulus configuration in the superficial layers of V1 (Lawrence et al., 2017; Marquardt et al., 2019; Petro & Muckli, 2016), which receive feedback information from other cortical areas.

To understand the V1 networks described here, joint fMRI and electrophysiological recordings are required. Several studies have shown an association between ultra-slow spontaneous fMRI fluctuations and the envelope of gamma-band neural activity (Nir et al., 2007; Scholvinck et al., 2010; Scheeringa et al., 2011; Mateo et al., 2017). Gamma-band activity could affect vasomotor oscillations in cortical surface pial arterioles, which in turn would influence arrival of oxyhemoglobin to cortical tissue, changing the fMRI signal (Mateo et al., 2017; Drew

et al., 2020). A seminal hypothesis (Gray et al., 1989) is that perceptual binding of contours is produced by the synchronous neuronal activity of neurons representing different aspects of the same object (Singer, 2021), although not all agree (Riesenhuber & Poggio, 1999). Neuronal synchronization in beta-band neural activity has also been proposed as a player in contour integration (Kermani et al., 2020).

One limitation of this study is the lack of eye-movement control. Eye movements would allow stimuli to stray in the visual field, thus blurring the retinotopic stimulus mapping. Furthermore, several rough approximations were used for calculating V1 vertex coordinates in the visual field. We used a population prior map (Benson & Winawer, 2018) instead of retinotopic mapping for each participant. Also, alignment of the cortical anatomy relied on the default FreeSurfer inter-subject surface registration (Fischl, 2012) instead of current, more accurate methods (MSMsulc and MSMALL, Coalson et al., 2018) Another limitation of the study was the absence of manipulations comparing the same stimuli when attention is deployed in different ways (Luck et al., 1997; Martínez et al., 2006), which would allow a more precise delineation of the contributions of exogenous and endogenous influences on V1 network topology. A caveat for future applications is that the methods outlined here are optimal for block design studies in which temporal separation between experimental conditions is guaranteed. Furthermore, it would be wise to only compare conditions in which stimulus layout fluctuations over the retina are minimal.

Ideas and speculations

Several interesting extensions of our research immediately come to mind. Perceptual organization seems to sculpt V1 connectivity, with specific increases in link strengths (in an overall background of decreases). This could facilitate object recognition in noisy backgrounds,

help break camouflage, and direct object-based attention. The neural basis of Gestalt laws of perceptual organization could be explored with our methods. Also, changes in V1 network topology associated with different interpretations of ambiguous (Wyatte et al., 2014) or multi-stable figures (Li et al., 2017) could be studied. Furthermore, as mentioned above, V1 networks could be compared for different attentional strategies when observing the same stimuli (Flevaris & Robertson, 2011; Luck et al., 1997). Additionally, the effects of changes in canonical object orientation (that modify configural processing) could be examined. (e.g., upright vs. inverted faces (Strother et al., 2011)). It would also be interesting to compare the network membership of V1 nodes that map the interior of illusory surfaces with those mapping the inducing stimuli (S. Chen et al., 2020; Keane et al., 2021). In all these questions, ultrahigh-field fMRI studies with cortical-layer specific recordings could improve our understanding of the mechanisms generating intra-V1 connectivity (Huber et al., 2020; Marquardt et al., 2019; Petro & Muckli, 2017). Granger causality or mediation analysis could be used to separate the role of lateral interactions in V1 from feedback influence from higher-order areas. Lastly, further experiments in the outlined directions will be facilitated by the software tools in this article.

Conclusions

V1 networks, estimated from background fMRI activity, reflect the perceptual organization of observed visual scenes, with stable topologies across individuals. Although these networks' spatial resolution is coarse compared to microelectrode unit recordings in monkeys (and obviously, they will be blind to faster neuronal interactions), they speak to a finer scale than seen in ROI-based networks. Furthermore, their visualization benefits from the close correspondence between retinotopy and anatomy found in V1. V1 networks are easy to estimate in human experiments and could occupy an intermediate level of analysis, perhaps analogous to

546 the relation of fMRI-based pRFs relative to microelectrode-measured RFs. The main appeal of
547 studying intra-V1 networks is that it may allow indirect but precise visualization of cooperative
548 effects among higher-order visual areas, otherwise hidden in voxels scattered across the cortex.
549

Materials and Methods

Participants

Twenty-six human volunteers aged from 23 to 28 years (9 females) participated in the study. All had normal or corrected-to-normal vision, did not present any medical condition and were right-handed except for two cases. The ethics committee of the University for Electronic Science and Technology of China (UESTC) approved the procedures, and participants gave written informed consent following the Helsinki declaration.

Task and stimuli

This experiment is described in more detail in (Valdés-Sosa et al., 2020b). The stimuli were projected on a screen at the subject's feet, viewed through an angled mirror fixed to the MRI head-coil, and were generated using the Cogent Matlab toolbox (http://www.vislab.ucl.ac.uk/cogent.php). Modified Global and Local Navon letters, made from white lines on a black background (Figure 1A), alternated with a baseline matrix of (about 2.0° wide and 5.3° high). This matrix was built out of smaller placeholder elements shaped like '8's (with visual angles about 40' wide and 1° 3' high). Two letters' E' and 'U' were presented at both levels. Blocks consisted of ten 1 sec repetitions of the same letter (within a fixed level), that alternated with 1 sec baseline periods thus lasting 20 s. Blocks were initiated by a cue ('Global' or 'Local'), followed by a 19-sec baseline, and ended with a 4-sec wait period where counts of small deviations in letter shape were reported. Four or five runs were presented, each consisting of 12 blocks.

Data acquisition and Image preprocessing

Data acquisition and initial image preprocessing are described in detail in (Valdés-Sosa et al., 2020b). Recordings was carried out with a GE Discovery MR750 3T scanner (General

573 Electric Medical Systems, Milwaukee, WI, USA) using an 8 channel receiver head coil. A T1-
574 weighted image was obtained with 1 x 1 x 0.5 mm resolution. A mid-gray surface was
575 reconstructed from the T1 image for each subject using Freesurfer
576 (http://surfer.nmr.mgh.harvard.edu), registered to the FsAverage template, and subsampled to
577 81924 vertices. Discs with 5mm radii were defined over the FsAverage surface using the Surfing
578 toolbox (http://surfing.sourceforget.net). The T1 image was also segmented and normalized to
579 MNI space using SPM12. For each subject, masks of white matter and cerebrospinal fluid (CSF)
580 were created using a threshold of tissue probability greater than 0.9, and the CSF mask was
581 restricted to the ventricles using a template in MNI space (the
582 https://sites.google.com/site/mrilateralventricle/template).

583 Functional images were obtained with a T2*- weighted echo planar imaging sequence
584 (TR=2.5s; TE =40 ms; flip angle=90°). Spatial resolution was 1.875 x 1.875 x 2.9, with 135
585 images per run. The initial 5 volumes in all runs were discarded to stabilize T1 magnetization.
586 Pre-preprocessing of functional data included artifact correction, slice-timing, head motion
587 correction (with extraction of motion parameters) and unwarping using ArtRepair toolbox
588 (http://cibsr.stanford.edu/tools/ArtRepair/ArtRepair.htm) and SPM8
589 (http://www.fil.ion.ucl.ac.uk/spm/). Next, the fMRI time series were projected to each individual
590 mid-gray cortical surface and high-pass filtered with a time constant of 128 s.

591 Analysis of fMRI activity

592 Background activity was defined as the residual time series of each surface vertex after
593 regressing out the effects of the stimuli (evoked response) and 64 nuisance parameters using the
594 general linear model (GLM). The nuisance regressors included the six primary motion
595 parameters (obtained from head motion correction), along with their derivatives, and the

quadratics of both these sets (24 motion regressors in total). Physiologic noise was modelled using the aCompCor method (Behzadi et al., 2007) on the time series extracted separately from the white matter and the ventricles masks described above. The first five principal components from each set of time series, the derivatives of these components, and the quadratics of all these parameters were obtained (40 regressors in total). Therefore, the nuisance regressors totalled 64 parameters. We applied a univariate general linear model with the vertex-wise fMRI time series as dependent variables in four variants, and the residuals as the output. In the first variant (no-deconvolve), only nuisance regressors were included in the design matrix (i.e., the stimulus response was not eliminated). In another variant (canonical-HRF), the stimulation block was modelled as a square wave convolved with the canonical hemodynamic function. In the last variant a FIR basis (18 stick functions for 45 s, about the duration of a complete stimulus cycle) was used. As a control, the power spectra of the complete times series were extracted for each individual and averaged over participants.

After applying the GLM, the time series were segmented into blocks considering the time shift introduced by the hemodynamic function. These segments were linearly detrended. Segments corresponding to the same stimulus were concatenated. The background activity from surface vertex was smoothed by averaging with the time series of its neighbors in the 5 mm discs mentioned above. For this article, only activity from vertices in the V1 region corresponding to the central 8 degrees of eccentricity of a population prior map of retinotopy (Benson & Winawer, 2018) were used. Different vertices could be missing due to noise or BOLD signal dropout in each case.

Analysis of V1 connectivity

Pearson correlation coefficient matrices in V1 were calculated for each participant and stimulus condition and transformed to z values using the Fisher transformation. Negative correlations were set to zero, and missing values in each subject's correlation matrix were substituted by the median value of the other subjects without missing values. Within-subjects two-tailed Student's t-tests were calculated based on the differences between connectivity matrices associated with the stimulus conditions in each experiment. Statistical thresholds, considering multiple comparison corrections, were estimated by controlling the False Discovery Rate (Fdr) at a level of q = 0.05 (two-tailed). To compute the FDR (Bielczyk et al., 2018), we used mixture models to estimate the Null (H0) and the alternative distributions (H1s) from the histogram of observed t-values. Four mixture models were fit using expectation-maximization: a) Only a Gaussian-H0; b) The Gaussian H0 plus a negative gamma H1 distribution; c) the Gaussian-H0 plus a positive gamma H1 distribution; d) And the Gaussian-H0 plus negative gamma and positive gamma H1 distributions. The model with lowest Bayesian Information Criterion (BIC) was selected as the best fit (Gorgolewski et al., 2012). The FDR was calculated for each t-value (on the right tail) as the area above the observed t-value under the H1 distribution, relative to the number of counts of the histogram (which reflects the contribution of both H0 and H1), and correspondingly for the left tail. The minimum t-value in the right tail associated with an FDR smaller than q (or the maximum value for the left tail) was defined as the threshold. In some cases, some of these thresholds did not exist.

The geodesic distance between V1 cortical sites was calculated with the Fast Marching toolbox (https://es.mathworks.com/matlabcentral/fileexchange/6110-toolbox-fast-marching)

based on the FsAverage surface for each cortical hemisphere. The curve fit MATLAB toolbox was used to fit the Fisher-transformed correlations as a function of geodesic distance.

Analysis of V1 connectivity in the visual space

The mean polar angle and eccentricity were extracted for V1 cortical vertices from a population prior map (Benson & Winawer, 2018). Edges that were significant in the statistical tests were depicted in graph plots in visual field coordinates. The color of lines in the graph plot represented either the t-tests surviving the FDR thresholds or Cohen's d binned according to effect strength. The length of these lines was measured in visual degrees, and the difference in distributions between experimental conditions was assessed with a Kruskal-Wallis test.

Eleven sub-networks (connSubsp) of the intra-V1 connectivity matrix were defined 'a-priori" (illustrated in the top row of Figure 7). The number of connections falling into each sub-network was counted and displayed in histograms, and contrasts between conditions were carried out by Fisher's exact test. The cNBS methodology (Noble and Scheinost, 2020) was used to perform network-level statistical tests of the contrasts between the Global and Local conditions. Observed and resampled (n=1000) edgewise t-values were averaged within each connSubsp sub-network (the distributions of t-values were centered by subtracting their mean). Resampling consisted of flipping the signs of the observed t-values over participants. A p-value for each the observed t-value in each group was calculated from the null distribution produced by resampling. The cNBS was also recalculated by bootstrapping 1000 times over participants and the mean and standard deviations of the resulting distributions were used to calculate Cohen's d.

Dimensionality

To estimate statistical dimensionality for fMRI data, we used the 'participation ratio' (Litwin-Kumar et al., 2017), as used by Ito et al (Ito et al., 2020). Here we obtained the

covariance matrices for each stimulus period, and for the corresponding preceding baseline, and extracted the eigenvalues associated with each of them. Roughly explained, the participation ratio finds the number of eigenvalues needed to explain variance greater than a given threshold, thus more components indicating a higher dimensionality of the data. The measures of dimensionality were submitted to an analysis of variance.

Bibliography

Årup, F., Kai, L., & Goutte, Cyril; Nielsen, Finn Årup; Hansen, L. K. (2000). *Modeling the Haemodynamic Response in fMRI Using Smooth FIR Filters*. https://doi.org/10.1109/42.897811

Baldassano, C., Fei-Fei, L., & Beck, D. M. (2016). Pinpointing the peripheral bias in neural scene processing networks during natural viewing. *Journal of Vision*, *16*(2), 9. https://doi.org/10.1167/16.2.9.doi

Baldassano, C., Iordan, M. C., Beck, D. M., & Fei-Fei, L. (2012). Voxel-level functional connectivity using spatial regularization. *NeuroImage*, *63*(3), 1099–1106. https://doi.org/10.1016/j.neuroimage.2012.07.046

Barbot, A., Xue, S., & Carrasco, M. (2021). Asymmetries in visual acuity around the visual field. *Journal of Vision*, *21*(1), 1–23. https://doi.org/10.1167/JOV.21.1.2

Behzadi, Y., Restom, K., Liau, J., & Liu, T. T. (2007). A component based noise correction method (CompCor) for BOLD and perfusion based fMRI. *NeuroImage*, *37*(1), 90–101. https://doi.org/10.1016/j.neuroimage.2007.04.042

Benson, N. C., Butt, O. H., Datta, R., Radoeva, P. D., Brainard, D. H., & Aguirre, G. K. (2012). The retinotopic organization of striate cortex is well predicted by surface topology. *Current Biology : CB*, *22*(21), 2081–2085. https://doi.org/10.1016/j.cub.2012.09.014

Benson, N. C., & Winawer, J. (2018). Bayesian analysis of retinotopic maps. *ELife*, *7*, 1–29. https://doi.org/10.7554/elife.40224

Bielczyk, N. Z., Walocha, F., Ebel, P. W., Haak, K. v., Llera, A., Buitelaar, J. K., Glennon, J. C., & Beckmann, C. F. (2018). Thresholding functional connectomes by means of mixture

690 modeling. *NeuroImage*, *171*(October 2017), 402–414.
691 https://doi.org/10.1016/j.neuroimage.2018.01.003
692 Bijsterbosch, J., Harrison, S. J., Jbabdi, S., Woolrich, M., Beckmann, C., Smith, S., & Duff, E. P.
693 (2020). Challenges and future directions for representations of functional brain
694 organization. *Nature Neuroscience*, *23*(12), 1484–1495. https://doi.org/10.1038/s41593-
695 020-00726-z
696 Bijsterbosch, J., Smith, S., & Beckmann, C. (2017). *Introduction to resting state fMRI functional*
697 *connectivity*.
698 Bock, A. S., Binda, P., Benson, N. C., Bridge, H., Watkins, K. E., & Fine, I. (2015). Resting-
699 State Retinotopic Organization in the Absence of Retinal Input and Visual Experience.
700 *Journal of Neuroscience*, *35*(36), 12366–12382. https://doi.org/10.1523/JNEUROSCI.4715-
701 14.2015
702 Briggs, F. (2020). Role of Feedback Connections in Central Visual Processing. *Annual Review of*
703 *Vision Science*, *6*, 313–334. https://doi.org/10.1146/annurev-vision-121219-081716
704 Chen, G., Shin, Y. W., Taylor, P. A., Glen, D. R., Reynolds, R. C., Israel, R. B., & Cox, R. W.
705 (2016). Untangling the relatedness among correlations, part I: Nonparametric approaches to
706 inter-subject correlation analysis at the group level. *NeuroImage*, *142*, 248–259.
707 https://doi.org/10.1016/j.neuroimage.2016.05.023
708 Chen, G., Taylor, P. A., Stoddard, J., Cox, R. W., Bandettini, P. A., & Pessoa, L. (2022). Sources
709 of Information Waste in Neuroimaging: Mishandling Structures, Thinking Dichotomously,
710 and Over-Reducing Data. *Aperture Neuro*, *2021*(5), 1–22.
711 https://doi.org/10.52294/2e179dbf-5e37-4338-a639-9ceb92b055ea

Chen, M., Yan, Y., Gong, X., Gilbert, C. D., Liang, H., & Li, W. (2014). Incremental Integration of Global Contours through Interplay between Visual Cortical Areas. *Neuron*, *82*(3), 682–694. https://doi.org/10.1016/j.neuron.2014.03.023

Chen, S., Weidner, R., Zeng, H., Fink, G. R., Müller, H. J., & Conci, M. (2020). Tracking the completion of parts into whole objects: Retinotopic activation in response to illusory figures in the lateral occipital complex. *NeuroImage*, *207*(June 2019), 116426. https://doi.org/10.1016/j.neuroimage.2019.116426

Christiaan Klink, P., Chen, X., Vanduffel, W., & Roelfsema, P. R. (2021). Population receptive fields in non-human primates from whole-brain fmri and large-scale neurophysiology in visual cortex. *ELife*, *10*, 1–35. https://doi.org/10.7554/eLife.67304

Christman, S. D. (1993). Local-global processing in the upper versus lower visual fields. *Bulletin of the Psychonomic Society*, *31*(4), 275–278. https://doi.org/10.3758/BF03334927

Chung, J., Bridgeford, E., Arroyo, J., Pedigo, B. D., Saad-Eldin, A., Gopalakrishnan, V., Xiang, L., Priebe, C. E., & Vogelstein, J. T. (2021). Statistical connectomics. *Annual Review of Statistics and Its Application*, *8*, 463–492. https://doi.org/10.1146/annurev-statistics-042720-023234

Coalson, T. S., Van Essen, D. C., & Glasser, M. F. (2018). The impact of traditional neuroimaging methods on the spatial localization of cortical areas. *Proceedings of the National Academy of Sciences of the United States of America*, *115*(27), E6356–E6365. https://doi.org/10.1073/pnas.1801582115

Cole, M. W., Ito, T., Cocuzza, C., & Sanchez-Romero, R. (2021). The functional relevance of task-state functional connectivity. *Journal of Neuroscience*, *41*(12), 2684–2702. https://doi.org/10.1523/JNEUROSCI.1713-20.2021

Dawson, D. A., Lam, J., Lewis, L. B., Carbonell, F. M., Mendola, J. D., & Shmuel, A. (2016). Partial Correlation-Based Retinotopically Organized Resting-State Functional Connectivity Within and Between Areas of the Visual Cortex Reflects More Than Cortical Distance. *Brain Connectivity*, *6*(1), 57–75. https://doi.org/10.1089/brain.2014.0331

DeValois, R. L., & DeValois, K. K. (1991). Spatial Vision. In *Oxford Psychology Series*. https://doi.org/10.1093/acprof:oso/9780195066579.001.0001

Field, D. J., & Hayes, A. (2004). Contour Integration and the Lateral Connections of V1 Neurons. In *The Visual Neurosciences* (pp. 1096--1079).

Fischl, B. (2012). FreeSurfer. *NeuroImage*, *62*(2), 774–781. https://doi.org/10.1016/j.neuroimage.2012.01.021

Flevaris, A. v, Bentin, S., & Robertson, L. C. (2010). Local or global? Attentional selection of spatial frequencies binds shapes to hierarchical levels. *Psychological Science*, *21*(3), 424–431. https://doi.org/10.1177/0956797609359909

Flevaris, A. v, & Robertson, L. C. (2011). *Attentional selection of relative SF mediates global versus local processing : Evidence from EEG*. *11*, 1–12. https://doi.org/10.1167/11.7.11.Introduction

Flevaris, A. v., & Robertson, L. C. (2016). Spatial frequency selection and integration of global and local information in visual processing: A selective review and tribute to Shlomo Bentin. *Neuropsychologia*, *83*, 192–200. https://doi.org/10.1016/j.neuropsychologia.2015.10.024

Goodale, M. A., & Milner, A. D. (2018). Two visual pathways – Where have they taken us and where will they lead in future? *Cortex*, *98*, 283–292. https://doi.org/10.1016/j.cortex.2017.12.002

757 Gorgolewski, K. J., Storkey, A. J., Bastin, M. E., & Pernet, C. R. (2012). Adaptive thresholding
758 for reliable topological inference in single subject fMRI analysis. *Frontiers in Human*
759 *Neuroscience*, *6*(AUGUST), 1–14. https://doi.org/10.3389/fnhum.2012.00245
760 Gravel, N., Harvey, B., Nordhjem, B., Haak, K. V., Dumoulin, S. O., Renken, R., Ćurčić-Blake,
761 B., & Cornelissen, F. W. (2014). Cortical connective field estimates from resting state fMRI
762 activity. *Frontiers in Neuroscience*, *8*(OCT), 1–10.
763 https://doi.org/10.3389/fnins.2014.00339
764 Gray, C. M., König, P., Engel, A. K., & Singer, W. (1989). Oscillatory responses in cat visual
765 cortex exhibit inter-columnar synchronization which reflects global stimulus properties.
766 *Nature*, *338*(6213), 334–337. https://doi.org/10.1038/338334a0
767 Haak, K. V., & Beckmann, C. F. (2016). Objective analysis of the topological organization of the
768 human cortical visual connectome suggests three visual pathways. *Cortex*, 1–11.
769 https://doi.org/10.1016/j.cortex.2017.03.020
770 Haak, K. V., Winawer, J., Harvey, B. M., Renken, R., Dumoulin, S. O., Wandell, B. A., &
771 Cornelissen, F. W. (2013). Connective field modeling. *NeuroImage*, *66*, 376–384.
772 https://doi.org/10.1016/j.neuroimage.2012.10.037
773 Han, S., & Humphreys, G. W. (2010). *The Quarterly Journal of Experimental Psychology*
774 *Section A : Human Experimental Psychology Segmentation and selection contribute to local*
775 *processing in hierarchical analysis*. *November 2012*, 37–41.
776 Han, S., Humphreys, G. W., & Chen, L. (1999). Parallel and competitive processes in
777 hierarchical analysis: perceptual grouping and encoding of closure. *Journal of Experimental*
778 *Psychology. Human Perception and Performance*, *25*(5), 1411–1432.
779 https://doi.org/10.1037/0096-1523.25.5.1411

Han, S., Weaver, J. A., Murray, S. O., Kang, X., Yund, E. W., & Woods, D. L. (2002). Hemispheric asymmetry in global/local processing: Effects of stimulus position and spatial frequency. *NeuroImage*, *17*(3), 1290–1299. https://doi.org/10.1006/nimg.2002.1255

Harrison, S. A., & Tong, F. (2009). Decoding reveals the contents of visual working memory in early visual areas. *Nature*, *458*(7238), 632–635. https://doi.org/10.1038/nature07832

Huber, L., Finn, E. S., Chai, Y., Goebel, R., Stirnberg, R., Stöcker, T., Marrett, S., Uludag, K., Kim, S. G., Han, S. H., Bandettini, P. A., & Poser, B. A. (2020). Layer-dependent functional connectivity methods. *Progress in Neurobiology*, *May*, 101835. https://doi.org/10.1016/j.pneurobio.2020.101835

Iglesias-Fuster, J., Santos-Rodríguez, Y., Trujillo-Barreto, N., & Valdés-Sosa, M. J. (2014). Asynchronous presentation of global and local information reveals effects of attention on brain electrical activity specific to each level. *Frontiers in Psychology*, *5*(OCT), 1–14. https://doi.org/10.3389/fpsyg.2014.01570

Ito, T., Brincat, S. L., Siegel, M., Mill, R. D., He, B. J., Miller, E. K., Rotstein, H. G., & Cole, M. W. (2020). Task-evoked activity quenches neural correlations and variability across cortical areas. In *PLoS Computational Biology* (Vol. 16, Issue 8 August). https://doi.org/10.1371/JOURNAL.PCBI.1007983

Jiang, Y., & Han, S. (2005). Neural mechanisms of global/local processing of bilateral visual inputs: an ERP study. *Clinical Neurophysiology : Official Journal of the International Federation of Clinical Neurophysiology*, *116*(6), 1444–1454. https://doi.org/10.1016/j.clinph.2005.02.014

Kapadia, M. K., Ito, M., Gilbert, C. D., & Westheimer, G. (1995). Improvement in visual sensitivity by changes in local context: Parallel studies in human observers and in V1 of alert monkeys. *Neuron*, *15*(4), 843–856. https://doi.org/10.1016/0896-6273(95)90175-2

Kay, K. N., David, S. V., Prenger, R. J., Hansen, K. A., & Gallant, J. L. (2008). Modeling low-frequency fluctuation and hemodynamic response timecourse in event-related fMRI. *Human Brain Mapping*, *29*(2), 142–156. https://doi.org/10.1002/hbm.20379

Kay, K. N., Weiner, K. S., & Grill-Spector, K. (2015). Attention reduces spatial uncertainty in human ventral temporal cortex. *Current Biology*, *25*(5), 595–600. https://doi.org/10.1016/j.cub.2014.12.050

Keane, B. P., Barch, D. M., Mill, R. D., Silverstein, S. M., Krekelberg, B., & Cole, M. W. (2021). Brain network mechanisms of visual shape completion. *NeuroImage*, *236*. https://doi.org/10.1016/j.neuroimage.2021.118069

Keller, A. S., Jagadeesh, A. v., Bugatus, L., Williams, L. M., & Grill-Spector, K. (2022). Attention enhances category representations across the brain with strengthened residual correlations to ventral temporal cortex. *NeuroImage*, *249*(January), 118900. https://doi.org/10.1016/j.neuroimage.2022.118900

Kermani, M., Zavitz, E., Oakley, B., Price, N. S. C., Hagan, M. A., & Wong, Y. T. (2020). Long-range neural coherence encodes stimulus information in primate visual cortex. *BioRxiv*. https://doi.org/10.1101/2020.06.22.164269

Kimchi, R., Yeshurun, Y., Spehar, B., & Pirkner, Y. (2016). Perceptual organization, visual attention, and objecthood. *Vision Research*, *126*, 34–51. https://doi.org/10.1016/j.visres.2015.07.008

Kuai, S. G., Li, W., Yu, C., & Kourtzi, Z. (2017). Contour Integration over Time: Psychophysical and fMRI Evidence. *Cerebral Cortex*, *27*(5), 3042–3051. https://doi.org/10.1093/cercor/bhw147

Kupers, E. R., Carrasco, M., & Winawer, J. (2019). Modeling visual performance differences 'around' the visual field: A computational observer approach. *PLoS Computational Biology*, *15*(5), 1–29. https://doi.org/10.1371/journal.pcbi.1007063

Lamme, V. A. F., & Roelfsema, P. R. (2000). The distinct modes of vision offered by feedforward and recurrent processing. *Trends in Neurosciences*, *23*(11), 571–579. https://doi.org/10.1016/S0166-2236(00)01657-X

Lawrence, S. J. D. D., Formisano, E., Muckli, L., Lange, F. P. De, & de Lange, F. P. (2017). Laminar fMRI: Applications for cognitive neuroscience. *NeuroImage*, *March*, 1–7. https://doi.org/10.1016/j.neuroimage.2017.07.004

Levine, M. W., & Mcanany, J. J. (2005). *The relative capabilities of the upper and lower visual hemifields*. *45*, 2820–2830. https://doi.org/10.1016/j.visres.2005.04.001

Li, H.-H., Rankin, J., Rinzel, J., Carrasco, M., & Heeger, D. J. (2017). Attention model of binocular rivalry. *Proceedings of the National Academy of Sciences*, *114*(30), E6192–E6201. https://doi.org/10.1073/pnas.1620475114

Liang, H., Gong, X., Chen, M., Yan, Y., Li, W., & Gilbert, C. D. (2017). Interactions between feedback and lateral connections in the primary visual cortex. *Proceedings of the National Academy of Sciences of the United States of America*, *114*(32), 8637–8642. https://doi.org/10.1073/pnas.1706183114

Litwin-Kumar, A., Harris, K. D., Axel, R., Sompolinsky, H., & Abbott, L. F. (2017). Optimal Degrees of Synaptic Connectivity. *Neuron*, *93*(5), 1153-1164.e7. https://doi.org/10.1016/j.neuron.2017.01.030

Luck, S. J., Chelazzi, L., Hillyard, S. a, & Desimone, R. (1997). Neural mechanisms of spatial selective attention in areas V1, V2, and V4 of macaque visual cortex. *Journal of Neurophysiology*, *77*(1), 24–42.

Markov, N. T., Misery, P., Falchier, A., Lamy, C., Vezoli, J., Quilodran, R., Gariel, M. A., Giroud, P., Ercsey-Ravasz, M., Pilaz, L. J., Huissoud, C., Barone, P., Dehay, C., Toroczkai, Z., Van Essen, D. C., Kennedy, H., & Knoblauch, K. (2011). Weight consistency specifies regularities of macaque cortical networks. *Cerebral Cortex*, *21*(6), 1254–1272. https://doi.org/10.1093/cercor/bhq201

Markov, N. T., Vezoli, J., Chameau, P., Falchier, A., Quilodran, R., Huissoud, C., Lamy, C., Misery, P., Giroud, P., Ullman, S., Barone, P., Dehay, C., Knoblauch, K., & Kennedy, H. (2014). Anatomy of hierarchy: Feedforward and feedback pathways in macaque visual cortex. *Journal of Comparative Neurology*, *522*(1), 225–259. https://doi.org/10.1002/cne.23458

Marquardt, I., de Weerd, P., Schneider, M., Gulban, O. F., Ivanov, D., & Uludağ, K. (2019). Depth-resolved ultra-high field fMRI reveals feedback contributions to surface motion perception. *BioRxiv*, 1–28. https://doi.org/10.1101/653626

Martínez, a, Teder-Sälejärvi, W., Vazquez, M., Molholm, S., Foxe, J. J., Javitt, D. C., di Russo, F., Worden, M. S., & Hillyard, S. a. (2006). Objects are highlighted by spatial attention. *Journal of Cognitive Neuroscience*, *18*(2), 298–310. https://doi.org/10.1162/089892906775783642

Nasr, S., Kleinfeld, D., & Polimeni, J. R. (2021). The Global Configuration of Visual Stimuli Alters Co-Fluctuations of Cross-Hemispheric Human Brain Activity. *The Journal of Neuroscience*, *41*(47), 9756–9766. https://doi.org/10.1523/jneurosci.3214-20.2021

Nasr, S., & Tootell, R. B. H. (2020). Asymmetries in global perception are represented in near-versus far-preferring clusters in human visual cortex. *Journal of Neuroscience*, *40*(2), 355–368. https://doi.org/10.1523/JNEUROSCI.2124-19.2019

Nastase, S. A., Gazzola, V., Hasson, U., & Keysers, C. (2019). Measuring shared responses across subjects using intersubject correlation. *Social Cognitive and Affective Neuroscience*, *14*(6), 669–687. https://doi.org/10.1093/scan/nsz037

Noble, S., Mejia, A. F., Zalesky, A., & Scheinost, D. (2022). Improving power in functional magnetic resonance imaging by moving beyond cluster-level inference. *Proceedings of the National Academy of Sciences*, *119*(32), e2203020119. https://doi.org/10.1073/PNAS.2203020119

Petro, L. S., & Muckli, L. (2016). The brain's predictive prowess revealed in primary visual cortex. *Proceedings of the National Academy of Sciences*, *113*(5), 1124–1125. https://doi.org/10.1073/pnas.1523834113

Petro, L. S., & Muckli, L. (2017). The laminar integration of sensory inputs with feedback signals in human cortex. *Brain and Cognition*, *112*, 54–57. https://doi.org/10.1016/j.bandc.2016.06.007

Pomerantz, J., & Portillo, M. (2012). Emergent features, gestalts, and feature integration theory. *From Perception to Consciousness: Searching with Anne Treisman*, 187–192. http://books.google.com/books?hl=en&lr=&id=f_NgRX1DJ7IC&oi=fnd&pg=PA187&dq=

Emergent+features,+gestalts,+and+feature+integration+theory&ots=QSjJw4inhL&sig=EmH80AVrRz6WZo0GoRm_ALkStKA

Previc, F. H. (1990). Functional specialization in the lower and upper visual fields in humans: Its ecological origins and neurophysiological implications. *Behavioral and Brain Sciences*, *13*(3), 519–542. https://doi.org/10.1017/S0140525X00080018

Raemaekers, M., Schellekens, W., van Wezel, R. J. A., Petridou, N., Kristo, G., & Ramsey, N. F. (2014). Patterns of resting state connectivity in human primary visual cortical areas: A 7T fMRI study. *NeuroImage*, *84*, 911–921. https://doi.org/10.1016/j.neuroimage.2013.09.060

Riesenhuber, M., & Poggio, T. (1999). Are cortical models really bound by the "binding problem"? *Neuron*, *24*(1), 87–93. https://doi.org/10.1016/S0896-6273(00)80824-7

Robertson, L. C., & Ivry, R. (2000). Hemispheric asymmetries: Attention to visual and auditory primitives. *Current Directions in Psychological Science*, *9*(2), 59–63. https://doi.org/10.1111/1467-8721.00061

Robertson, L. C., Ivry, R., & Robertson, L. C. (2010). *Attention Asymmetries : Hemispheric Visual and Auditory Primitives*. *9*(2), 59–63.

Roelfsema, P. R., & de Lange, F. P. (2016a). Early Visual Cortex as a Multiscale Cognitive Blackboard. *Annual Review of Vision Science*, *2*(1), 131–151. https://doi.org/10.1146/annurev-vision-111815-114443

Roelfsema, P. R., & de Lange, F. P. (2016b). Early Visual Cortex as a Multiscale Cognitive Blackboard. *Annual Review of Vision Science*, *2*(1), 131–151. https://doi.org/10.1146/annurev-vision-111815-114443

Sasaki, Y., Hadjikhani, N., Fischl, B., Liu, A. K., Marret, S., Dale, A. M., & Tootell, R. B. H. (2001). Local and global attention are mapped retinotopically in human occipital cortex.

Proceedings of the National Academy of Sciences, *98*(4), 2077–2082. https://doi.org/10.1073/pnas.98.4.2077

Schwarz, C., & Bolz, J. (1991). Functional specificity of a long-range horizontal connection in cat visual cortex: A cross-correlation study. *Journal of Neuroscience*, *11*(10), 2995–3007. https://doi.org/10.1523/jneurosci.11-10-02995.1991

Singer, W. (2021). Recurrent dynamics in the cerebral cortex: Integration of sensory evidence with stored knowledge. *Proceedings of the National Academy of Sciences*, *118*(33). https://doi.org/10.1073/pnas.2101043118

Smith, F. W., & Muckli, L. (2010). Nonstimulated early visual areas carry information about surrounding context. *Proceedings of the National Academy of Sciences of the United States of America*, *107*(46), 20099–20103. https://doi.org/10.1073/pnas.1000233107

Strother, L., Mathuranath, P. S., Aldcroft, A., Lavell, C., Goodale, M. A., & Vilis, T. (2011). Face inversion reduces the persistence of global form and its neural correlates. *PLoS ONE*, *6*(4). https://doi.org/10.1371/journal.pone.0018705

Tran, S. M., McGregor, K. M., James, G. A., Gopinath, K., Krishnamurthy, V., Krishnamurthy, L. C., & Crosson, B. (2018). Task-residual functional connectivity of language and attention networks. *Brain and Cognition*, *122*(January), 52–58. https://doi.org/10.1016/j.bandc.2018.02.003

Valdés-Sosa, M., Ontivero-Ortega, M., Iglesias-Fuster, J., Lage-Castellanos, A., Gong, J., Luo, C., Castro-Laguardia, A. M., Bobes, M. A., Marinazzo, D., & Yao, D. (2020a). Objects seen as scenes: Neural circuitry for attending whole or parts. *NeuroImage*, *210*(January). https://doi.org/10.1016/j.neuroimage.2020.116526

Valdés-Sosa, M., Ontivero-Ortega, M., Iglesias-Fuster, J., Lage-Castellanos, A., Gong, J., Luo, C., Castro-Laguardia, A. M., Bobes, M. A., Marinazzo, D., & Yao, D. (2020b). Objects seen as scenes: Neural circuitry for attending whole or parts. *NeuroImage*, *210*. https://doi.org/10.1016/j.neuroimage.2020.116526

Van Essen, D. C., Newsome, W. T., & Maunsell, J. H. R. (1984). The visual field representation in striate cortex of the macaque monkey: Asymmetries, anisotropies, and individual variability. *Vision Research*, *24*(5), 429–448. https://doi.org/10.1016/0042-6989(84)90041-5

Wagemans, J., Feldman, J., Gepshtein, S., Kimchi, R., Pomerantz, J. R., van der Helm, P. a, & van Leeuwen, C. (2012). A century of Gestalt psychology in visual perception: II. Conceptual and theoretical foundations. *Psychological Bulletin*, *138*(6), 1218–1252. https://doi.org/10.1037/a0029334

Wandell, B. A., & Winawer, J. (2015a). Computational neuroimaging and population receptive fields. *Trends in Cognitive Sciences*, *19*(6), 349–357. https://doi.org/10.1016/j.tics.2015.03.009

Wandell, B. A., & Winawer, J. (2015b). Computational neuroimaging and population receptive fields. *Trends in Cognitive Sciences*, *19*(6), 349–357. https://doi.org/10.1016/j.tics.2015.03.009

Williams, M. A., Baker, C. I., op de Beeck, H. P., Mok Shim, W., Dang, S., Triantafyllou, C., & Kanwisher, N. (2008). Feedback of visual object information to foveal retinotopic cortex. *Nature Neuroscience*, *11*(12), 1439–1445. https://doi.org/10.1038/nn.2218

Wyatte, D., Jilk, D. J., & O'Reilly, R. C. (2014). Early recurrent feedback facilitates visual object recognition under challenging conditions. *Frontiers in Psychology*, *5*(JUL), 1–10. https://doi.org/10.3389/fpsyg.2014.00674

Yukun, C. (2016). *Cortical feedback to V1 and V2 contains unique information about high-level scene structure. Authors: 44*(0), 1–29.

Author contributions

Designed research; MVS, MOO

Contributed analytic tools: MVS, MOO, ALC, PVS

Analyzed data: MVS, MOO, JIF

Wrote the paper: MVS, MOO, JIF, PVS

Competing Interests

The authors declare no competing interests.

Acknowledgements

We thank the University of Electronic Science and Technology of China (UESTC) for funding and providing special equipment and facilities for this project. This work was supported by the VLIR-UOS project "A Cuban National School of Neurotechnology for Cognitive Aging", the National Fund for Science and Innovation of Cuba, and the National Natural Science Foundation of China (#81861128001) and the 1110 Project (B12027) of China. The authors are grateful to K. Uludag for suggestions on the manuscript.